Online ISSN 1848-3380, Print ISSN 0005-1144
ATKAFF 56(4), 443–453(2015)

Petar R. Matić, Aleksandar Ž. Rakić, Darko P. Marčetić, Slobodan N. Vukosavić

Improved Torque Control of High Speed Shaft-Sensorless Induction Motor Drive

DOI 10.7305/automatika.2016.01.852
UDK 681.532.65.073.09-83:621.313.33.072.2

Original scientific paper

This paper presents improved torque control scheme for a high speed sensorless induction motor drive. The proposed high speed torque control scheme substitutes the flux oriented control by the voltage angle control in the flux weakening regime. This scheme uses maximum of available inverter voltage, alleviates well known problems of current control schemes in conditions with insufficient voltage margin and avoids the influence of estimated speed error to the achieved flux level. The algorithm uses similar slip control as flux oriented control algorithm, but is applied without an outer flux trajectory reference which is typical for the flux weakening, providing a fast and well damped torque response even if error in estimated speed is present.

Experiments confirm the effectiveness of proposed torque control algorithm, smooth transition from the flux oriented control in the base speed region to the voltage angle control in the flux weakening, superior dynamic performance of the voltage angle torque control, and its robustness to an estimated rotor speed error.

Key words: High Speed Induction Motor, Toque Control, Voltage Angle Control

Unaprijeđeno upravljanje momentom visokobrzinskog pogona s asinkronim motorom bez mjerenja brzine. U radu je predstavljena unaprijeđena shema upravljanja za pogon visokobrzinskog asinkronog motora bez mjerenja brzine. Predloženi postupak zamjenjuje vektorsko upravljanje upravljačkom strukturom s upravljanjem kutom napona u slabljenju polja. Predložena shema koristi maksimalni raspoloživi napon invertora, eliminira dobro poznate probleme strujno reguliranih pogona u uvjetima s nedovoljnom rezervom napona i eliminira utjecaj greške u estimaciji brzine na dostignutu razinu toka. Algoritam koristi sličnu kontrolu klizanja kao i vektorsko upravljanje, ali bez tipičnog vanjskog zadavanja toka u slabljenju polja, pružajući brz i dobro prigušen odziv momenta čak i u slučaju greške u estimaciji brzine.

Eksperimenti izvedeni na velikoj brzini vrtnje potvrđuju učinkovitost predložene regulacije momenta, gladak prijelaz iz baznog područja brzine u slabljenje polja, vrhunske dinamičke performanse upravljanja kutom napona i robusnost na pogrešku u estimiranoj brzini vrtnje.

Ključne riječi: Visokobrzinski asinnkroni motor, Upravljanje momentom, Kontrola kuta napona

1 INTRODUCTION

Torque and flux control in Induction Motor (IM) drives is commonly achieved through the Field Oriented Control (FOC), which is based on decoupling of the torque-producing and flux-producing components of stator current vector, or through the Direct Torque Control (DTC), which is based on a direct control of stator voltage without inner current control loop [1, 2]. In IM drives torque and flux are coupled and they are controlled simultaneously by using fast current regulated inverters (in FOC drives), or by employing hysteresis controllers or decoupling circuits (in DTC drives). In both cases respective flux components are kept constant in base speed region, and decreased above the base speed in flux weakening region [3].

Medium and high-speed induction machines gain attention due to better efficiency, larger power-to-weight ratio, and smaller size and cost. They can be used without mechanical gear in wide speed range and mainly operate in flux weakening [4-8]. In order to achieve maximum torque capability in flux weakening, a torque control algorithm that fully utilizes available inverter voltage is mandatory [9-11]. For proper operation of the inner current loops in the FOC scheme a minimum voltage margin has to be preserved. The margin is obtained by reducing the flux and/or using over modulation, but with lowering the flux under the optimal level or producing harmonics. If the flux reference is given in inverse proportion to the shaft speed, the torque dynamics is than dependent both on the current regulator dynamics and mechanical time constant [12-15]. The absence of an explicit current controller in DTC

scheme insures better DC bus utilization then in FOC [16-19]. The most of the FOC and DTC schemes accomplish torque control by using outer flux trajectories calculated from the steady state relations without modeling machine dynamics.

Additional problem with the low cost drives operating at ultra high speeds is the estimation accuracy of the model outputs (such is rotor speed) and states (such are flux vector and torque). First of all, in order to keep the overall price of drive low, phase voltage estimation and phase currents reconstruction from single DC link shunt is performed. Also, because of the fact that fundamental frequencies of high speed machines are in the range of few hundreds of hertz, which cannot be followed with the increase of Pulse Width Modulation (PWM) frequency, low fundamental to estimator sampling frequency ratio is expected. That gives rise of new problems that result in inaccurate flux position and speed estimation [20] which highly influence FOC performance in flux weakening.

The proposed torque control scheme is combination of the best properties of FOC at low speeds and Voltage Angle Torque Control (VATC) at high speeds. Algorithm obtains fast and well damped torque response in the full speed range. In the base speed region torque is controlled by stator currents in the Indirect FOC (IFOC) structure, while in the flux weakening regime torque is controlled by VATC structure with smooth transition between these two modes. The VATC algorithm supplies the machine with full constant voltage in the flux weakening and the outer flux trajectory reference is not necessary because torque control loop automatically adjusts the rotor flux level [21]. This approach enables full utilization of both magnetic material of the machine and power capabilities of the inverter. The algorithm does not need the precise knowledge of the flux position and therefore is robust against an error in estimated speed. Also, the algorithm avoids usage of inner current control loops in voltage limit and thus is robust against supply voltage fluctuation.

In the Section 2 mathematical IM models for the IFOC control in the base speed region and the VATC model for control at high speeds are given. Adequate tunings of the PI regulator with variable gains for the VATC control are proposed in order to obtain well damped torque response in the flux weakening regime. The proposed torque control scheme is presented in the Section 3. The scheme is based on the approach presented in [22], but upgraded with the low speed IFOC and smooth transition between the IFOC to the VATC modes. It is shown that unique control structure can be used both for the base speed region (when machine operates in the IFOC mode) and in the flux weakening (when machine operates in the VATC mode). The smooth transition from the base speed region to the flux weakening region is provided by holding the output voltage components at the values achieved in the IFOC mode and keeping them constant in the VATC mode. By this, the control is switched from the current control to the voltage angle control without changing the control structure, calculating the base speed or employing outer flux reference trajectories. In the VATC mode motor dynamics variations are compensated for by using torque regulator with variable gains. In the Section 4 experimental verification of the static and dynamic performance in the torque and the speed control modes, as well as robustness against estimated speed error is given. Section 5 is the Conclusion.

2 IFOC AND VATC TORQUE CONTROL OF IM

Mathematical model of the IM in synchronous rotating reference frame is given in equations (1) through (6),

$$\overrightarrow{u}_{\mathrm{s}}=r_{\mathrm{s}}i_{\mathrm{s}}+\frac{1}{\omega_{\mathrm{b}}}\frac{\mathrm{d}\overrightarrow{\Psi}_{\mathrm{s}}}{\mathrm{d}t}+\mathrm{j}\omega_{\mathrm{e}}\overrightarrow{\Psi}_{\mathrm{s}}, \tag{1}$$

$$0=r_r i_r+\frac{1}{\omega_b}\frac{\mathrm{d}\overrightarrow{\Psi}_r}{\mathrm{d}t}+\mathrm{j}\left(\omega_e-\omega_r\right)\overrightarrow{\Psi}_r, \tag{2}$$

$$\overrightarrow{\Psi}_s=l_s\overrightarrow{i}_s+l_m\overrightarrow{i}_r, \tag{3}$$

$$\overrightarrow{\Psi}_r=l_r\overrightarrow{i}_r+l_m\overrightarrow{i}_s, \tag{4}$$

$$t_{\mathrm{e}}=-\mathrm{Im}\left\{\overrightarrow{\Psi}_s\overrightarrow{i}_{\mathrm{s}}\right\}, \tag{5}$$

$$T_{\mathrm{m}}\frac{\mathrm{d}\omega_{\mathrm{r}}}{\mathrm{d}t}=t_{\mathrm{e}}-t_l, \tag{6}$$

where $\overrightarrow{u}_s$, $\overrightarrow{i}_s$ are the stator voltage and current vectors in [p.u.], $\rightarrow_s, \rightarrow_r$, are the stator and rotor flux vectors in [p.u.], ω_e, ω_r are the synchronous and rotor angular speed in [p.u], ω_b is the model base speed [rad/s], l_s, l_r, r_s, r_r are the stator and rotor inductance and resistance [p.u], l_m is the mutual inductance in [p.u], t_e, t_l are the IM and load torque in [p.u], and T_m is mechanical time constant [s].

In the base speed region, both synchronous speed ω_e and stator voltage modulus vary with torque and speed, while the rotor flux is kept constant. In the flux weakening region, stator voltage modulus is kept constant, synchronous speed varies with the torque and speed, while the rotor flux must be changed.

In the flux weakening regime, the stator voltage is limited due to a limited DC bus voltage U_{DC}. In terms of *dq* components, the voltages u_d and u_q are limited by

$$|\overrightarrow{u}_{\mathrm{s}}|=\sqrt{u_{\mathrm{d}}^2+u_{\mathrm{q}}^2}\leq U_{\mathrm{s}} \tag{7}$$

where $U_s = U_{DC}/\sqrt{3}$ is the peak phase voltage available.

2.1 IFOC torque control in the base speed region

In the base speed region available voltage is sufficient and decoupled torque and flux control is obtained by proper orientation of the synchronous reference frame and by current supply (IFOC control). For the machine fed from current source, and synchronous reference frame d_1q_1 aligned with the rotor flux ($\left|\overrightarrow{\Psi}_{\mathrm{rd}}\right|=\Psi_{\mathrm{rd1}}$, $\Psi_{\mathrm{rq1}}=0$) as shown in Fig. 1, the IM model is:

$$\frac{\mathrm{d}\Psi_{\mathrm{rd1}}}{\mathrm{d}t}+\frac{1}{T_{\mathrm{r}}}\Psi_{\mathrm{rd1}}=\frac{l_{\mathrm{m}}}{T_{\mathrm{r}}}i_{\mathrm{sd1}}, \tag{8}$$

$$t_{\mathrm{e}}=\frac{l_{\mathrm{m}}}{l_{\mathrm{r}}}\Psi_{\mathrm{rd1}}i_{\mathrm{sq1}}, \tag{9}$$

$$\omega_{sl}=\frac{l_m}{T_r\Psi_{rd1}}i_{sq1}, \tag{10}$$

$$\vartheta_{d1q1}=\int(\omega_{sl}+\omega_r)\,\mathrm{d}t, \tag{11}$$

where ϑ_{d1q1} is the synchronous reference frame orientation angle and ω_{sl} is the slip angular speed [p.u].

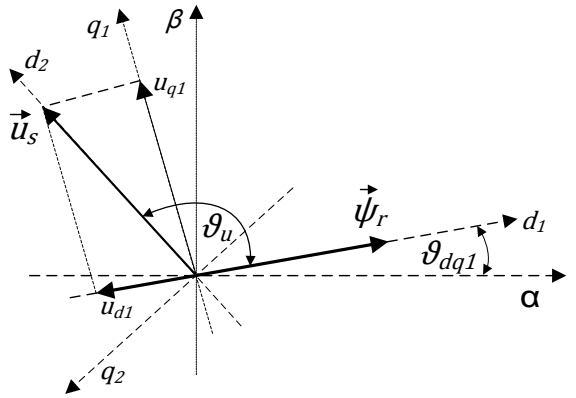

Fig. 1. Synchronous reference frames $\boldsymbol{d_1q_1}$ and $\boldsymbol{d_2q_2}$.

The orientation of the synchronous reference frame d_1q_1 is calculated using (10) and (11) and in the IFOC mode rotor flux and torque are controlled independently.

2.2 VATC Torque Control in the Flux Weakening

In order to fully utilize DC bus voltage, the second synchronous reference frame d_2q_2 is aligned with the stator voltage $\overrightarrow{u}_s$ ($u_{d2}=U_s$, $u_{q2}=0$), as shown in Fig. 1. When the stator voltage amplitude is limited, the only control variable in model (1-6) is the voltage angle ϑ_u proportional to the synchronous speed ω_e:

$$\vartheta_{d2q2}=\vartheta_{d1q1}+\vartheta_u, \tag{12}$$

$$\vartheta_u=\pi-\arctan\frac{u_{q1}}{u_{d1}}\,. \tag{13}$$

In the voltage limit, the IM torque can be controlled by voltage angle control without outer flux reference [21]. Linearized model is derived from (1-7) assuming that stator dynamics is much faster than rotor and mechanical dynamics. The approximated transfer function is obtained for the least favorable pole position, i.e. for the unloaded IM as given in [22]. The IM transfer function obtained by linearization around operating point "0" is given as:

$$G_{t_e}(p)=G_0\frac{\frac{p}{\omega_z}+1}{\frac{p^2}{\omega_{nr}^2}+\frac{2\xi_r p}{\omega_{nr}}+1}. \tag{14}$$

The static gain G_0, transfer function zero's frequency ω_z, rotor poles' natural frequency ω_{nr}, and damping ratio ξ_r are given as functions of synchronous speed:

$$G_0=\frac{k_sk_rT_r^{'}\left(U^0T_s^{'}\right)^2}{\sigma L_s\left(\left(\omega_{d2q2}^0T_s^{'}\right)^2+\left(1-k_sk_r\right)^2\right)}, \tag{15}$$

$$\omega_z=\frac{\omega_b}{T_r^{'}}\frac{\left(\omega_{d2q2}^0T_s^{'}\right)^2+\left(1-k_sk_r\right)^2}{\left(\left(\omega_{d2q2}^0T_s^{'}\right)^2+\left(1+T_s^{'}/T_r^{'}\right)\left(1-k_sk_r\right)\right)}, \tag{16}$$

$$\omega_{nr}=\frac{\omega_b}{T_r^{'}}\sqrt{\frac{\left(\omega_{d2q2}^0T_s^{'}\right)^2+\left(1-k_sk_r\right)^2}{1+\left(\omega_{d2q2}^0T_s^{'}\right)^2}}, \tag{17}$$

$$\xi_r=\frac{\left(\omega_{d2q2}^0T_s^{'}\right)^2+1-k_sk_r}{\sqrt{1+\left(\omega_{d2q2}^0T_s^{'}\right)^2}\sqrt{\left(\omega_{d2q2}^0T_s^{'}\right)^2+\left(1-k_sk_r\right)^2}}, \tag{18}$$

where $k_s=l_m/l_s$, $k_r=l_m/l_r$ are stator and rotor coupling coefficients, $\sigma=1-l_m^2/(l_sl_r)$ is leakage coefficient, $T_s^{'}=\sigma l_s/r_s$ and $T_r^{'}=\sigma l_r/r_r$ are stator and rotor transient time constants in [p.u].

In flux weakening, further approximations can be used:

$$\omega_{d2q2}^0T_s^{'}\gg\left(1-k_sk_r\right), \tag{19}$$

$$\frac{\left(\omega_{d2q2}^0T_s^{'}\right)^2}{1+\left(\omega_{d2q2}^0T_s^{'}\right)^2}\approx 1, \tag{20}$$

and steady-state gain (15) takes shorter form:

$$G_0 \approx \frac{k_s k_r T_r^{'}}{\sigma l_s}\left(\frac{U^0}{\omega_{d2q2}^0}\right)^2, \tag{21}$$

zero's (16) and poles' natural frequency (17) overlap:

$$\omega_z \approx \omega_{nr} \approx \frac{\omega_b}{T_r^{'}}, \tag{22}$$

and model (15-18) simplifies to:

$$G_{te}\left(p\right)=\frac{k_s k_r T_r^{'}}{\sigma l_s}\left(\frac{U^0}{\omega_{d2q2}^0}\right)^2 \frac{1}{\frac{\mathrm{p}}{\omega_b/T_r^{'}}+1}. \tag{23}$$

Motor torque, represented by simplified model (23), can be regulated by simple proportional – integral (PI) torque regulator, parameterized in the form:

$$K_{tePI}\left(p\right)=K_C\left(\frac{1}{\omega_C}+\frac{1}{p}\right), \tag{24}$$

where ω_C is desired closed-loop bandwidth and K_C is the regulator gain tuned to achieve it. Closed-loop bandwidth ω_C can be selected as high as the natural frequency (17) of rotor poles, in order to avoid non modeled high-frequency dynamics. The tunings of the PI regulator are:

$$\omega_C=\frac{\omega_b}{T_r^{'}}, \tag{25}$$

$$K_C=\frac{\omega_C}{G_0}=\frac{\omega_b \sigma l_s}{k_s k_r T_r^{'2}}\left(\frac{\omega_{d2q2}^0}{U^0}\right)^2. \tag{26}$$

It should be noted from (24)-(26) that the gains of the PI regulator change with the synchronous speed ω_e, i. e. gain scheduling is introduced. The gain scheduler (26) insures that the projected dynamics of VATC structure is preserved for any value of synchronous speed. If needed, the influence of the DC bus voltage variation to the VATC dynamic can also be eliminated by altering the value U^0 in (26).

3 PROPOSED TORQUE CONTROL SCHEME SUITABLE FOR BOTH BASE AND HIGH SPEED REGION

In the base speed region proposed torque control algorithm operates as the standard IFOC structure (8-11), while in the flux weakening regime operates as the VATC with gain scheduling. Transition between two modes is performed within the proposed unique control scheme without switches or additional nonlinearities.

3.1 Transition from IFOC to VATC Control Scheme

In the base speed region the IFOC structure provides control variables which are stator voltage components u_{d1} and u_{q1} and the angle ϑ_{d1q1}, shown in the Fig. 1. Both u_{d1} and u_{q1} depend on the flux and torque in the base speed region and increase with the speed. When the voltage limit (7) is reached, current regulators saturate, and IFOC control becomes unstable. Border values of voltage components u_{d1}^{LIM} and u_{q1}^{LIM} are

$$\sqrt{\left(u_{d1}^{LIM}\right)^2+\left(u_{q1}^{LIM}\right)^2}=U_s. \tag{27}$$

Once the voltage limit (27) is reached, the proposed control scheme abandons IFOC and switches to VATC with voltage amplitude U_s kept at maximum value. The initial voltage angle ϑ_u^{LIM} is defined by the ratio of the border voltage components u_{d1}^{LIM} and u_{q1}^{LIM}

$$\vartheta_u^{LIM}=\pi-\arctan\frac{u_{q1}^{LIM}}{u_{d1}^{LIM}} \tag{28}$$

valid at the beginning of the flux weakening region. With stator resistance neglected, the angle ϑ_u^{LIM} is:

$$\vartheta_u^{LIM} \approx \pi-\arctan\frac{i_{d1}}{\sigma i_{q1}}\ . \tag{29}$$

The initial voltage angle depends only on the i_{d1}/i_{q1} ratio, which confirms that smooth transition between IFOC and VATC modes can be is obtained for any values of the voltage, torque and the speed.

When the voltage limit is reached, the torque control is achieved by VATC with

$$u_{d2}=U_s=\sqrt{\left(u_{d1}^{LIM}\right)^2+\left(u_{q1}^{LIM}\right)^2}, \tag{30}$$

$$u_{q2}=0, \tag{31}$$

and the angle ϑ_{d2q2} as the only control variable shown in Fig 1. Torque control is achieved by regulating the slip frequency on the output of the torque PI regulator with gain scheduling. Adequate voltage angle is calculated as

$$\vartheta_{d2q2}=\int K_c\left(\omega_{sl}+\omega_r\right)\mathrm{d}t+\vartheta_u^{LIM}. \tag{32}$$

By comparing control angles in the base speed region (11) to flux weakening (32), and using (12), it can be seen that control strategy for both base speed and flux weakening regions can be expressed in only one reference frame and with only one torque regulator used in both structures. In the base speed region, control variables are stator voltages components, u_{d1}, u_{q1}, and the angle $\int\left(\omega_{sl}+\omega_r\right)dt$ from the IFOC. In the flux weakening, control variables are u_{d1}^{LIM}, u_{q1}^{LIM} and the angle $\int K_c\left(\omega_{sl}+\omega_r\right)dt$ provided by the VATC.

3.2 Block – Diagram of the Proposed Control Scheme

The proposed control scheme is depicted in Fig. 2. Torque reference t_e^* and magnetizing stator current reference i_d^* are the inputs. Torque is regulated by torque regulator which gives slip reference ω_{sl}^* at the output.

In the base speed region, torque producing stator current reference i_q^* is calculated from the reference slip and reference magnetizing current. Stator currents are regulated by PI regulators which give motor voltages u_d^* and u_q^*. The voltages are transformed from the synchronous to the phase reference frame and fed to the motor. Slip reference is limited to the break-down slip and added to the estimated rotor speed $\widehat{\omega}_r$.

The position of rotor flux vector ϑ_{dq} in the base speed region is obtained by integrating synchronous speed ω_{dq}. Estimated torque $\hat{t}_e$ and rotor speed $\widehat{\omega}_r$ are obtained from the phase voltages and currents. In the base speed region machine is supplied by stator currents and the diagram in Fig. 4 is common rotor flux oriented IFOC scheme. The output K_C (26) of the gain scheduling block (GS in Fig. 2) is limited at unity and is not effective.

In the flux weakening, current regulators are suspended and machine is voltage fed by the constant stator voltage components which are held in blocks H in Fig.2. By holding output voltages, control is switched from current control (ref. frame d_1q_1 in Fig. 1) to voltage control (ref. frame d_2q_2 in Fig.1). GS block becomes active, and the IFOC scheme from Fig. 2 reduces to the VATC scheme [22] shown in Fig. 3. When speed lower than the base speed threshold is reached, it is presumed that there is sufficient voltage margin for current regulators to operate, and IFOC mode is restored. Current regulators are activated, first with relaxed gains to ensure smooth transition from voltage to current controlled mode.

4 EXPERIMENTAL EVALUATION

Experimental verification is conducted on the laboratory set-up with high speed IM drive with parameters given in the Appendix. The IM was controlled with 3-phase voltage inverter, based on low cost fixed point DSP. Output currents were reconstructed from measurement on single shunt placed in the inverter DC circuit. Rotor speed was estimated using Model Reference Adaptive System (MRAS) [20]. Sample time and PWM switching frequency are set to be 16 kHz.

In order to verify dynamic performance of the proposed DTC torque control in the field weakening, the results are compared to common IFOC control in the field weakening, with outer magnetizing current i_d^* trajectory in form $1/\omega_r$ upgraded with current regulators voltage margin controller. Margin controller with anti-windup mechanism additionally decreases rotor flux if voltage margin less than 5% is sensed.

4.1 Transition from the Base Speed Region to Flux Weakening

In the first set of experiments the transition from the FOC in the base speed region to the VATC in the flux weakening region is closely examined. In the experiments the machine was accelerated from 2000 rpm to 8000 rpm in torque control mode, without outer speed regulator, which could mask torque dynamics. Three different torque references of 0.33 Nm, 0.66 Nm and 1 Nm in rectangular pulse shape are applied and results are shown in Figs 4−6: motor speed ω_r and torque T_e (a), slip speed ω_{sl} and output power P_{out} (b), stator currents i_d and i_q (c) and stator voltages u_d and u_q (d).

Motor starts accelerating in IFOC structure with constant flux command. In the case of T_e^*=0.33 Nm (Fig 4a) approx. at *t*=2.1s and around the rotor speed of 4343 rpm the rated voltage is reached. From this point on, control structure is switched to VATC. Slip speed (Fig 4b) increases due to gain scheduling mechanism from Fig. 3, while d axis current decreases (Fig 4c). Stator voltages u_d and u_q are captured and held constant throughout the whole flux weakening regime (Fig 4d). In that way smooth transition is achieved.

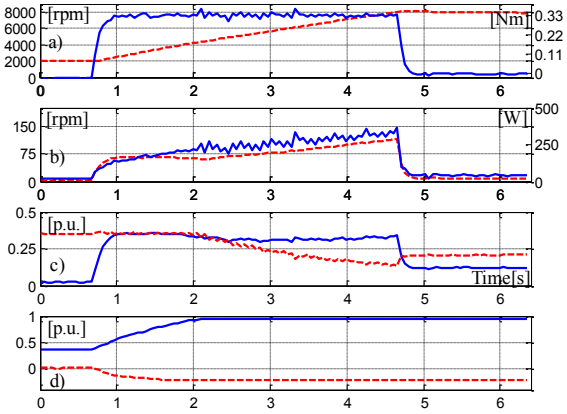

Fig. 4. Transition from IFOC to VATC, torque reference 0.33Nm. Motor speed $\boldsymbol{\omega_r}$ (dashed) and torque $\boldsymbol{t_e}$ (a), slip speed $\boldsymbol{\omega_{sl}}$ (dashed) and output power $\boldsymbol{P_{out}}$ (b), stator currents $\boldsymbol{i_d}$ (dashed) and $\boldsymbol{i_q}$ (c), stator voltages $\boldsymbol{u_d}$ (dashed) and $\boldsymbol{u_q}$ (d).

Figs 5 and 6 show that smooth transition from base speed region to flux weakening are obtained for larger torque references also. For torque reference of 0.66 Nm (Fig.5), the motor enters flux weakening regime at rotor speed of 3465 rpm, while for torque reference of 1Nm (Fig.6), flux weakening is entered at 3072 rpm.

Base speed, at which motor enters flux weakening regime depends on the load, i.e. machine reaches rated

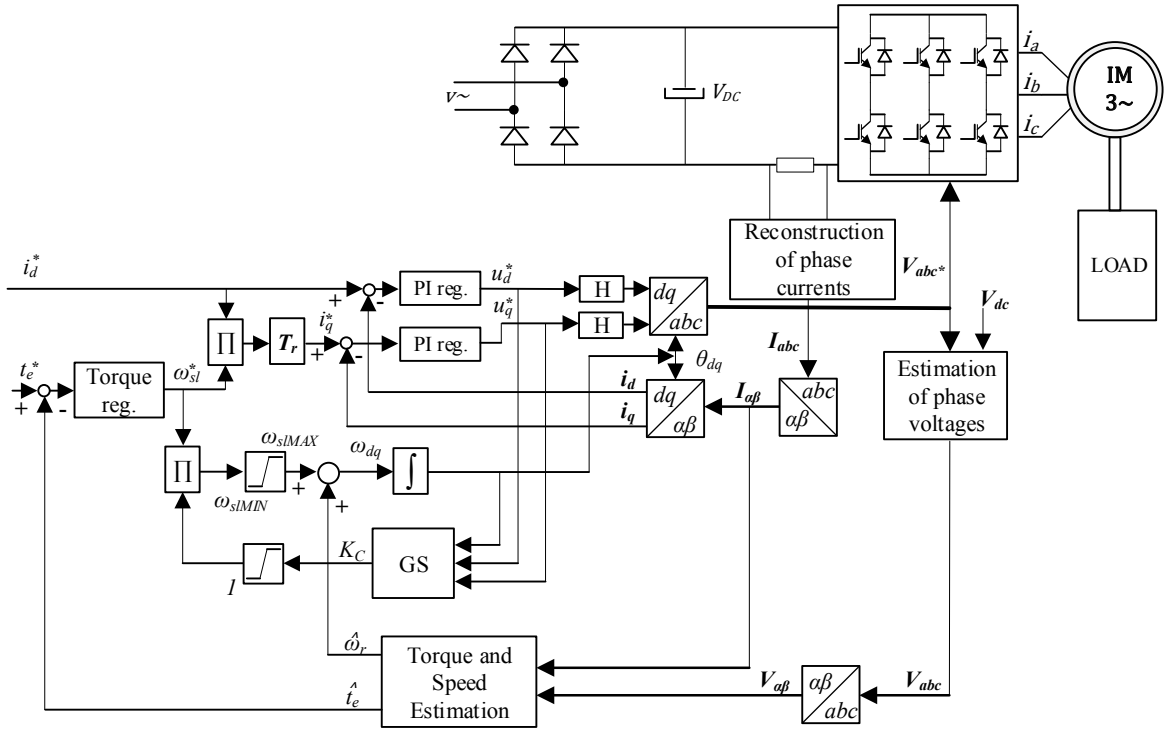

Fig. 2. Proposed torque control scheme valid for the full speed range

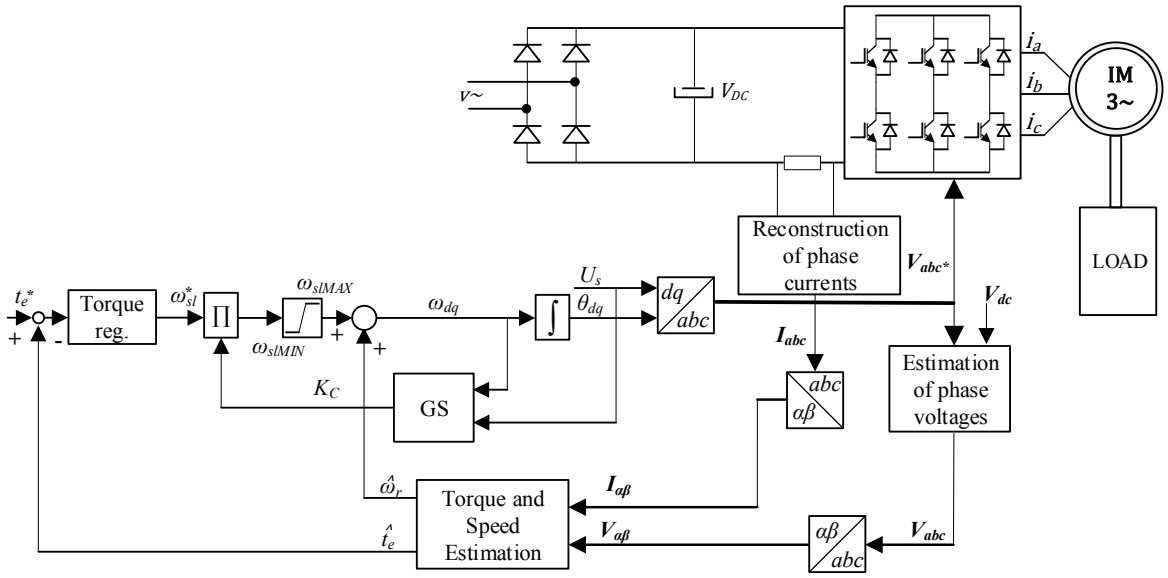

Fig. 3. Torque control scheme from Fig. 2 in the flux weakening region

voltage at lower speeds as load increases. In the proposed VATC algorithm, it is not necessary to calculate base speed, since flux weakening is entered automatically at the point when rated voltage is reached, and operating in flux weakening is performed without outer flux reference.

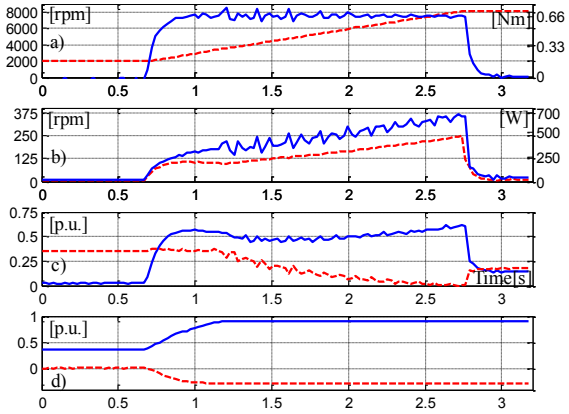

Fig. 5. Transition from IFOC to VATC, torque reference 0.66Nm. Motor speed ω_r (dashed) and torque t_e (a), slip speed ω_{sl} (dashed) and output power P_{out} (b), stator currents i_d (dashed) and i_q (c), stator voltages u_d (dashed) and u_q (d).

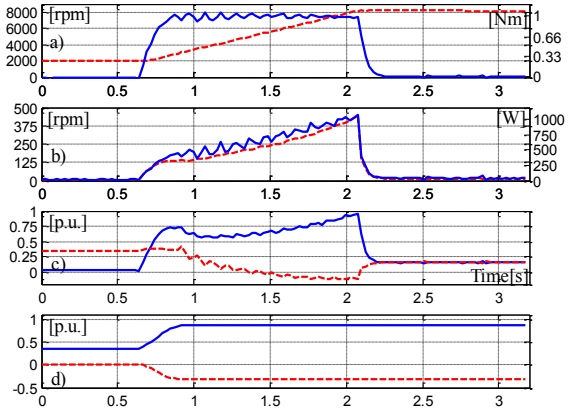

Fig. 6. Transition from IFOC to VATC, torque reference 1Nm. Motor speed ω_r (dashed) and torque t_e (a), slip speed ω_{sl} (dashed) and output power P_{out} (b), stator currents i_d (dashed) and i_q (c), stator voltages u_d (dashed) and u_q (d).

4.2 Torque Control in Deep Flux Weakening

In order to verify performance and robustness of the VATC and compare it with classic IFOC in the deep flux weakening, in the next set of experiments two torque pulses are applied in the sequence, Figs 7−9. During the first torque pulse motor accelerates from 8000 rpm to 12000 rpm. The second torque pulse is applied after 1 s pause and kept until motor further accelerates from 12000 rpm to 16000 rpm. Torque and speed (a), slip speed (b), stator current (c) stator voltage and rotor flux (d) are shown.

Torque reference is first set to 0.25 Nm (Fig. 7a). The VATC provides needed torque during the both acceleration periods in flux weakening. Slip speed increases (Fig 7b) as shaft speed increases, because rotor flux decreases (Fig. 7d).

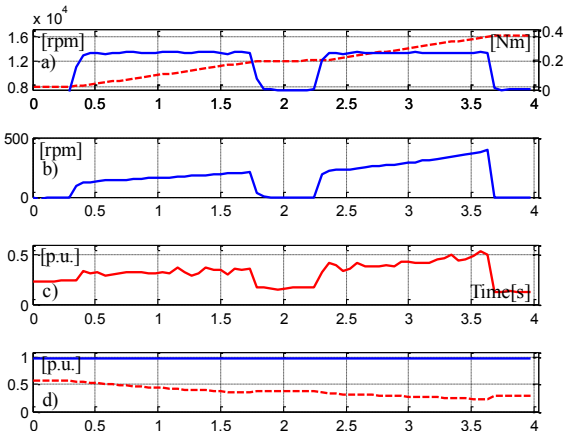

Fig. 7. VATC control scheme, torque reference 0.25Nm applied in pulses. Motor speed ω_r (dashed) and torque t_e (a), slip speed ω_{sl} (b), stator current amplitude (c), rotor flux Ψ_r (dashed), stator voltage amplitude U_s (d).

The same reference as shown in Fig. 7 is applied to IFOC control scheme. The results are shown in Fig. 8, from which it can be seen that IFOC structure cannot follow the second pulse reference due to lack of voltage.

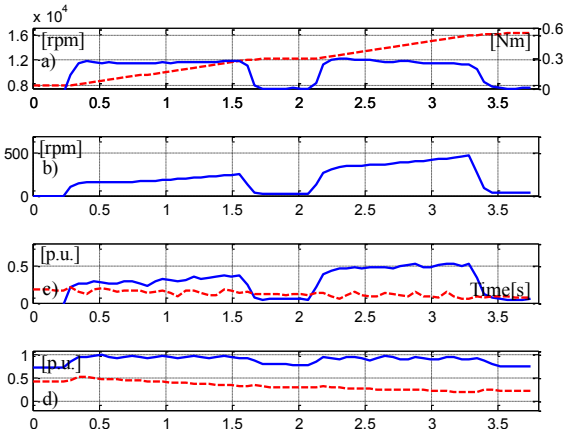

Fig. 8. IFOC control scheme, torque reference 0.25Nm applied in pulses. Motor speed ω_r (dashed) and torque t_e (a), slip speed ω_{sl} (b), stator current amplitude (c), rotor flux Ψ_r (dashed), stator voltage amplitude U_s (d).

Fig. 9 shows the regime when torque reference pulses are increased to 0.5Nm. The VATC scheme fully follows

the torque reference during the first torque pulse in lower speed range in flux weakening. During the second torque pulse, the slip enters to the slip limit of 600 rpm (Fig. 8b), and IM continues to operate with reduced torque output.

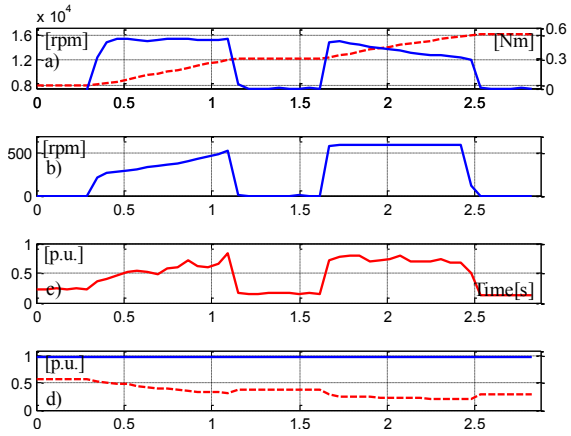

Fig. 9. VATC control scheme, torque reference 0.5Nm applied in pulses. Motor speed ω_r (dashed) and torque t_e (a), slip speed ω_{sl} (b), stator current amplitude (c), rotor flux Ψ_r (dashed), stator voltage amplitude U_s (d).

4.3 VATC Speed Control Mode in Flux Weakening

In this experiment, the performance of the VATC in field weakening with included outer speed loop based on simple PI regulator is investigated. Speed reference is set to 12000 rpm. The torque load step of 0.4 Nm is applied at 1s, and then removed at 5.2s (Fig. 10). Fig. 10a shows both measured and estimated speed, which are good match. Fig. 10b shows the inner torque loop response, while achieved slip speed and inverter output power are shown in Fig. 10c, d.

The experimental results confirm that rotor speed can be properly regulated by controlling the torque reference by the VATC scheme. The speed response is quite satisfying for most of high speed IM applications in field weakening.

4.4 Robustness of the Proposed VATC Torque Controller against Estimated Speed Error

In order to explore robustness of the VATC against estimated rotor speed error, the estimated rotor speed was artificially set to false values of +0.5% (Fig. 11) and -0.5% of actual speed (Fig. 12) for torque reference of 0.25Nm. Fig. 11 and Fig. 12 show that the VATC response does not deteriorate for given rotor speed errors. The consequence is that the relatively small absolute speed error is incorporated in resulting slip speed in order to provide needed synchronous speed.

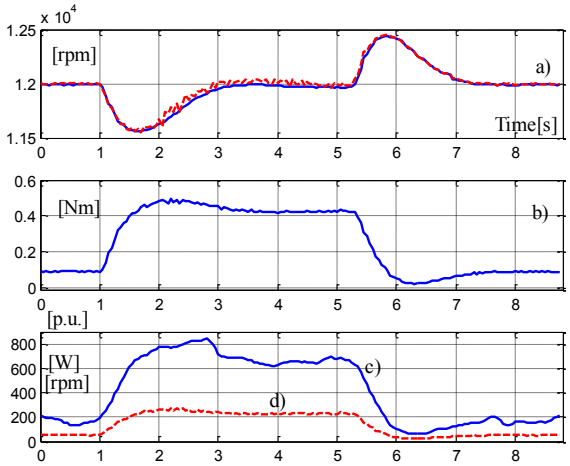

Fig. 10. Speed control mode with VATC control scheme. Estimated motor speed ω_r (dashed) and measured motor speed (solid) (a), motor torque t_e (b), output power P_{out} (dashed) and slip speed ω_{sl} (solid) (d).

The torque response in field weakening is compared with the response of IFOC sensorless control algorithm with the same references as for VATC and detuned estimated speed, Figs. 13 and 14.

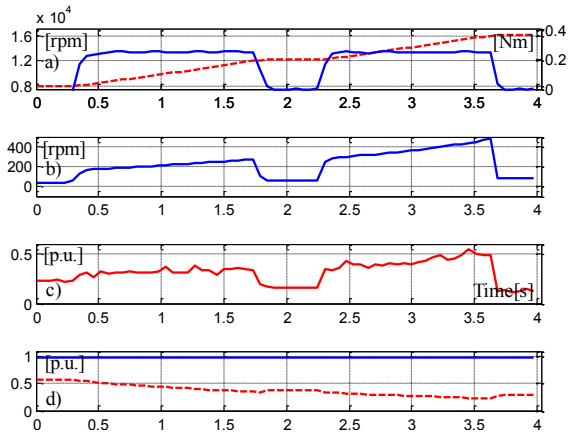

Fig. 11. VATC control scheme, torque reference 0.25Nm, speed error +0.5%. Motor speed ω_r (dashed) and torque t_e (a), slip speed ω_{sl} (b), stator current amplitude (c), rotor flux Ψ_r (dashed), stator voltage amplitude U_s (d).

Experimental results show that the VATC algorithm maintains similar torque response for different torque references and different speeds, which all is the result of proposed gain scheduling slip control with constant voltage applied. Also, results prove VATC robustness to the estimated speed error. VATC torque response is similar for

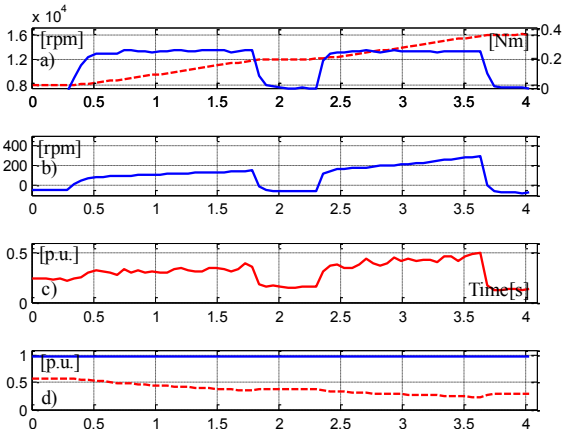

Fig. 12. VATC control scheme, torque reference 0.25Nm, speed error -0.5%. Motor speed ω_r (dashed) and torque t_e (a), slip speed ω_{sl} (b), stator current amplitude (c), rotor flux Ψ_r (dashed), stator voltage amplitude U_s (d).

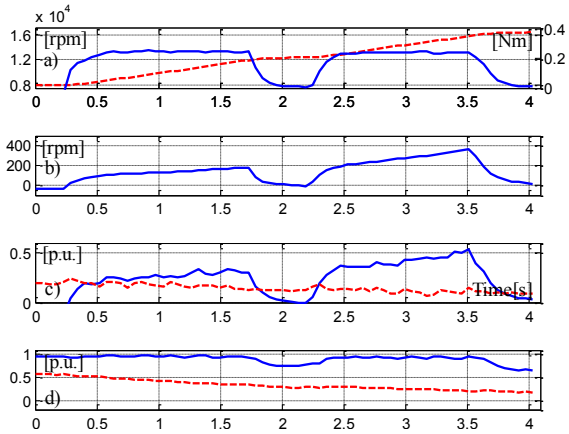

Fig. 14. IFOC control scheme, torque reference 0.25Nm, speed error -0.5%. Motor speed ω_r (dashed) and torque t_e (a), slip speed ω_{sl} (b), stator current amplitude (c), rotor flux Ψ_r (dashed), stator voltage amplitude U_s (d).

both +0.5% and -0.5% speed error. The only noticeable difference is in achieved slip speed by which VATC naturally compensates the speed error.

In contrast, IFOC scheme is incapable to achieve reference torque: for positive speed error the flux is higher and voltage margin is hit, while for negative error, the flux is lower and drive enters slip limit. Thus, IFOC is found to be very sensitive to speed estimation error. This sensitivity increases as ratio between i_d/i_q decreases.

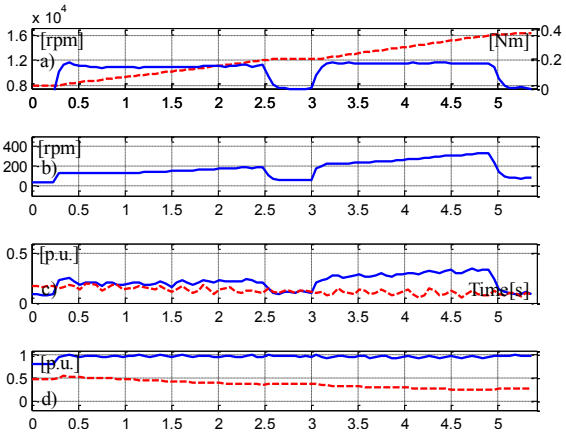

Fig. 13. IFOC control scheme, torque reference 0.25Nm, speed error +0.5%. Motor speed ω_r (dashed) and torque t_e (a), slip speed ω_{sl} (b), stator current amplitude (c), rotor flux Ψ_r (dashed), stator voltage amplitude U_s (d).

5 CONCLUSION

The torque control method proposed in this paper has target application in high speed sensorless IM drives working in deep flux weakening range with available voltage fully exploited. The method is designed as an extension of the IFOC torque control mode which becomes the VATC in the flux weakening. Experimental results prove that it is possible to have smooth transition between two modes at the start of flux weakening.

The results also show superior behavior of the new VATC scheme for different torques and speeds at different flux weakening levels. As a result, fast and well damped torque response is obtained. Proposed VATC algorithm in flux weakening is shown to be robust against speed estimation error. Additionally, the proposed VATC algorithm does not increase CPU time usage, increases robustness against estimated speed error, and eliminates the need for calculation the motor base speed.

APPENDIX A MOTOR DATA

Motor data: 750W, 195V, 70Hz, Rs=10.8Ω, Rr=5.673Ω, Ls=Lr=0.522H, Lm=0.518H, four poles.

REFERENCES

[1] D. Casadei, F. Profumo, G. Serra, A. Tani: "FOC and DTC: Two Viable Schemes for Induction Motor Torque Control", *IEEE Transactions on Power Electronics,* Vol. 17, No.5, September 2002, pp. 779-787.

[2] A. Sikorski, M. Korzeniewski:" Improved Algorithms of Direct Torque Control Method", *Automatika,* Vol. 54 (2013), No. 2, pp. 188-198.

[3] Lennart Harnefors, Kai Pietilainen, Lars Gertmar: "Torque – Maximizing Field-Weakening Control: Design, Analysis, and Parameter Selection", *IEEE Transactions on Industrial Electronics,* Vol. 48, No.1, February 2001.

[4] M. Ikeda, S. Sakabe, K. Higashi: "Experimental Study of High Speed Induction Motor Varying Rotor Core Construction, *IEEE Transactions on Energy Conversion*, Vol. 5, No. 1, March 1990, pp. 98–103.

[5] W. Soong: "Novel High-Speed Induction Motor for a Commercial Centrifugal Compressor," *IEEE Transactions on Industrial Applications*, Vol. 36, No. 3, May/Jun. 2000, pp. 706–713.

[6] J. Pyrhonen, J. Nerg, P. Kurronen, U. Lauber: " High-Speed High-Output Solid-Rotor Induction-Motor Technology for Gas Compression", *IEEE Transactions on Industrial Electronics*, Vol. 57, No.1, January 2010, pp. 272-280.

[7] M. Centner, U. Schäfer: "Optimized Design of High-Speed Induction Motors in Respect of the Electrical Steel Grade", *IEEE Transactions on Industrial Electronics*, Vol. 57, No.1, January 2010, pp. 288-295.

[8] J. F. Gieras, J. Saari: "Performance Calculation for a High-Speed Solid-Rotor Induction Motor", *IEEE Transactions on Industrial Electronics*, Vol. 59, No.6, June 2012, pp. 2689 - 2700

[9] M. Mengoni, L. Yarri, A. Tani, G. Serra, D. Casadei: "Stator Flux Vector Control of Induction Motor Drive in the Field Weakening Region", *IEEE Transactions on Power Electronics*, Vol. 23, No. 2, March 2008, pp. 941-949.

[10] P. Y. Lin, Y. S. Lai: "Novel Voltage Trajectory Control for Field-Weakening Operation of Induction Motor Drives", *IEEE Transactions on Industry Applications,* Vol. 47, No. 4, January/February 2011, pp. 122-127.

[11] R. Sepulchre, T. Devos, F. Jadot, F. Malrait: "Antiwindup Design for Induction Motor Control in the Field Weakening Domain", *IEEE Transactions on Control System Technology*, Vol. 21, No.1, January 2013, pp. 52-66.

[12] Fernando Briz, Alberto Diez, Micahel W. Degner, Robert D. Lorenz: "Current and Flux Regulation in Field – Weakening Operation", *IEEE Transactions on Industry Applications,* Vol. 37, No.1, January/February 2001, pp. 42-50.

[13] G. Gallegos-López, F. S. Gunawan, J. E. Walters: "Current Control of Induction Machines in the Field-Weakened Region", *IEEE Transactions on Industry Applications,* Vol. 43, No.4, July/August 2007, pp. 981-898.

[14] A. Tripathi, A. Khambadkone, S. Panda: "Dynamic Control of Torque in Overmodulation and in the Field Weakening Region", *IEEE Transactions on Power Electronics*, Vol. 21, No. 4, July 2006, , pp. 1091-1098.

[15] A. B. Jidin, N. R. B. Idris, A. H. B. M. Yatim, M. E. Elbuluk, T. Sutkino: „A Wide-Speed High Torque Capability Utilizing Overmodulation Strategy in DTC of Induction Machines With Constant Switching Frequency Controller", *IEEE Transactions on Power Electronics*, Vol. 27, No. 5, May 2012, pp. 2566-2575.

[16] D. Casadei, G. Serra, A. Tani, L. Zarri, F. Profumo: "Performance Analysis of a Speed Sensorless Induction motor Drive Based on a Constant Switching Frequency DTC Scheme", *IEEE Transactions on Industry Applications,* Vol. 39, No. 2, March/April 2003.

[17] T. Geyer, G. Papafotiou, M. Morari: "Model Predictive Direct Torque Control—Part I: Concept, Algorithm, and Analysis", *IEEE Transactions on Industrial Electronics*, Vol. 56, No.6, June 2009, pp. 1894-1905.

[18] M. Hajian, J. Soltani, G. A. Markadeh, S. Hosseinnia: "Adaptive Nonlinear Direct Torque Control of Sensorless IM Drives With Efficiency Optimization" *IEEE Transactions on Industrial Electronics,* Vol. 57, No.3, March 2010, pp. 975-985.

[19] J. Rodríguez, R. M. Kennel, J. R. Espinoza, M. Trincado, C. A. Silva, C. A. Rojas: "High-Performance Control Strategies for Electrical Drives: An Experimental Assessment", *IEEE Transactions on Industrial Electronics*, Vol. 59, No.2, February 2012, pp. 812-820.

[20] D. P. Marcetic, I. R. Krcmar, M. A. Gecic, P. R. Matic: „Discrete Rotor Flux and Speed Estimators for High Speed Shaft-Sensorless IM Drives", *IEEE Transactions on Industral Electronics,* Vol. 61, No. 6, June 2014, pp. 3099-3108.

[21] P. Matic, S. N. Vukosavic: "Direct Torque Control of Induction Motor in Field Weakening Without Outer Flux Trajectory Reference", *International Review of Electrical Engineering*, Vol. 6, No.3, June 2011.

[22] P. Matic, S. N. Vukosavic: "Voltage Angle Direct Torque Control of Induction Machine in Field Weakening Regime", *IET Electric Power Applications,* Volume 5, Issue 5, May 2011, pp. 404-414.

Petar R. Matić received the B.Sc. and M.S. degree from the University of Novi Sad, in 1999 and 2002, and Ph.D. degree from the Electrical Engineering Faculty, University of Belgrade, in 2011. Since 1999, he is with the Faculty of Electrical Engineering, University of Banja Luka, Bosnia and Herzegovina, teaching courses in electrical machines and drives. His scientific work is related to electrical machines and drives.

Aleksandar Ž. Rakić received the M.S. and Ph.D degree from the University of Belgrade in 2000 and 2010, respectively. Since 2001 he has been affiliated with the University of Belgrade, School of Electrical Engineering, where he is currently Assistant Professor, teaching courses in conventional and advanced control. His research interests include control design in electrical drives, power electronics, unmanned aerial vehicles, distributed and networked systems, as well as advanced metering and customer-side systems within the smart grid.

Darko P. Marčetić received the M.S. and Ph.D. degree from the Electrical Engineering Faculty, University of Belgrade, 1998 and 2006. In the period 2000-2006, he was with Motor Technology Center, Emerson Electric, St. Louis, MO and Emerson Appliance Controls, Elgin, IL, designing low-cost AC drives. Since 2006 he is with University of Novi Sad, teaching course in digital control of electrical drives. His research areas are power electronics and motor control.

Slobodan N. Vukosavić received his Ph.D. degree from the University of Belgrade in 1989. He was with the Nikola Tesla Institute until 1988, when he joined the Emerson Electric-ESCD. Since 1991, he was with Vickers Electric Company in Milan, and with MOOG Electric since 1994. He is currently Professor with the Electrical Engineering Department, University of Belgrade. He published over 70 papers, wrote 3 textbooks, 7 monographs and completed over 40 projects.

AUTHORS' ADDRESSES

Petar Matić,
University of Banja Luka,
Faculty of Electrical Engineering,
5 Patre,
78 000 Banja Luka, RS
Bosnia and Herzegovina
email: petar.matic@etfbl.net

Aleksandar Rakić, Slobodan Vukosavić,
University of Belgrade,
School of Electrical Engineering,
Bulevar Kralja Aleksandra 73,
11 000 Belgrade, Serbia
email: rakic@etf.rs, boban@etf.rs

Darko Marčetić,
University of Novi Sad,
Faculty of Technical Sciences,
Trg D. Obradovica 4,
21 000 Novi Sad, Serbia,
darmar@uns.ac.rs

Received: 2014-04-29
Accepted: 2014-12-29